arXiv:1303.4024v3 [cond-mat.supr-con] 20 May 2013

Low-energy magnetic defects in Fe-based superconductors

S. N. Khan,[1,2] Aftab Alam,[2] and Duane D. Johnson[1,2,3*]
[1]*Department of Physics, University of Illinois, Urbana-Champaign, Illinois 61801, USA*
[2]*The Ames Laboratory, US Department of Energy, Ames, Iowa 50011-3020, USA; and*
[3]*Department of Materials Science & Engineering, Iowa State University, Ames, Iowa 50011-2300.*
(Dated: May 22, 2013)

In Fe-pnictides, structural and magnetic planar defects proliferate over differing length scales, affecting descriptions of magnetism and superconductivity. "Ordered" Fe moments (0.8–1.04 μ_B) assessed by neutron scattering in the antiferromagnetic state are half the $\sim$1.6 μ_B from density-functional theory (DFT), while local probes are closer to DFT – a puzzle not yet understood. We study via DFT the stability and magnetic properties of competing antiphase and domain boundaries, twins, and isolated *nano*twins (equivalent to a twin nuclei), which exhibit low moments confined near defect boundaries. A single local-moment picture is thus inappropriate for long-range magnetic order. The nanoscale defects are very low energy (starting at 22 mJ/m^2), but twins remain so at the mesoscale, as observed, and our estimated distances between twins coincide with the observed magnetic correlation length. *Nano*twins also explain features in measured pair distribution functions. All these defects can be weakly mobile and/or have fluctuations that will lower assessed "ordered" moments from longer spatial and/or time averaging.

PACS numbers: 74.20.-z, 74.25.Ha, 75.25.-j, 75.30.Kz

Fe-based superconductors (FeSCs) are providing new means to understand unconventional superconductivity. Due to its ease of synthesis, $BaFe_2As_2$ has been chosen as a prototype for these systems, where its low-temperature (T $<$ 140 K) ground state is a striped, antiferromagnetic (AFM) orthorhombic ($Fmmm$) structure,[1] often called a spin-density wave (SDW), and which is reproduced in DFT calculations. At Neél T$_N$ (140 K), both a magnetic and structural transition occurs to a tetragonal ($I4/mmm$) paramagnet.[1] By doping with a transition-metal on the Fe-site, superconductivity (SC) can be achieved, and similarly with pressure.[2–4] There are strong connections between the magnetism and SC. Dopants weaken the magnetic state and Cooper pairing is, perhaps, driven by increased magnetic fluctuations out of the ground state.[5,6] Fermi-surface (FS) nesting is apparent from DFT calculations and agrees with angle-resolved photoemission (ARPES), suggesting an itinerant nature[7–9] and which is supported from the spin-wave dispersion.[10] Furthermore, DFT explains quantitatively effects of doping on FS nesting, and why Cu doping behaves differently than Co and Ni.[11] $K_xFe_2Se_2$ (isostructural to $BaFe_2As_2$) does not have the hole pockets needed for FS nesting,[12] as DFT finds.[13] Also, local, multi-orbital models yield a correct groundstate with a $s^{\pm}$ pairing symmetry for the gap function.[14,15] So, magnetism may be a result of itinerant or local electronic interactions,[16] with the likely description in between, indicated by measured fluctuating moments $\langle m^2\rangle \approx 3.2\ \mu_B^2$ that are much less than that given by Hund's rule.[17] Our analysis of magnetic defects also supports this conclusion, where we find locality and multiple magnetic states at defect boundaries. DFT results for $BaFe_2As_2$ also show a strong coupling between the structure and magnetism.[7,18] We explore this by varying the structural parameters in the presence of magnetic defects.

While DFT supports the observed SDW for the parent compound, the Fe moment ($1.6-1.9\ \mu_B$)[19,20] is twice that assessed for the average "ordered" moment from neutron diffraction ($0.8-1.04\ \mu_B$).[21–23] In fact, various experiments assess very different Fe moments. Core-electron spectroscopy[24] finds 2.1 μ_B, like DFT, while ^{57}Fe Mössbauer[1] and nuclear magnetic resonance[25] find 0.81 μ_B, as in diffraction assessments. For Fe-based magnets such a large discrepancy between ordered moments from theory and experiment is unusual. DFT+DMFT results show that there is large range in values of Hubbard U (0.5–4 eV) depending on the number of bands included;[26] nonetheless, due to Fe($3d$)-As($4p$) hybridization, the electronic structure is weakly correlated[16,26] and this agrees with x-ray and photoemission spectra.[26] Spin-orbit and hybridization (controlled by Fe/As planar spacing) in a U-based model was used to explain the small in-plane moments in Fe-pnictides.[27] Yet, our DFT moments are reduced $\sim$10% from spin-orbit, but 50-100% by slightly reduced Fe-As spacing. Also, a Bogoliubov-de Gennes model[28] suggests that only a large U induces domain walls. Yet, our results show that there are many low-energy magnetic defects, some with quenched moments, even without invoking smaller Fe-As spacings.

Nonetheless, spin fluctuations are agreed to play a big role, especially those involving magnetic planar defects, i.e., antiphase (APBs) and 90^o domain (DBs) boundaries (Figs. 1 and 2). Such defects have been proposed as key to any moment description,[29] but have yet to be quantitatively tested. With orthorhombic distortions ($a > b$), structural and concomitant magnetic twins, see Fig. 2, are observed in $BaFe_2As_2$ along $\langle 110\rangle$ with 10-50 μm between boundaries,[30] or much less 100-400 nm.[31] With stress samples detwin, but twins return upon its removal.[32] As in $YBa_2Cu_3O_{7-\delta}$,[33] $(1\bar{1}0)$ twins terminate on (110) twins. These defects cause anisotropic

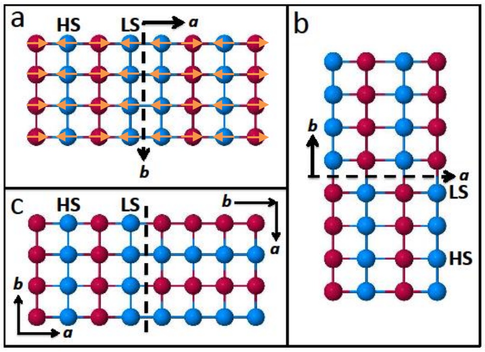

FIG. 1: (Color online) APB in the (a) *bc*-, (b) *ac*- planes, and (c) 90^o DB with no strain (a=b). Red (blue) circles are "up" ("down") in-plane moments, as indicated in (a). HS, MS and LS indicate Fe-sites with high-, medium- and low-spin states.

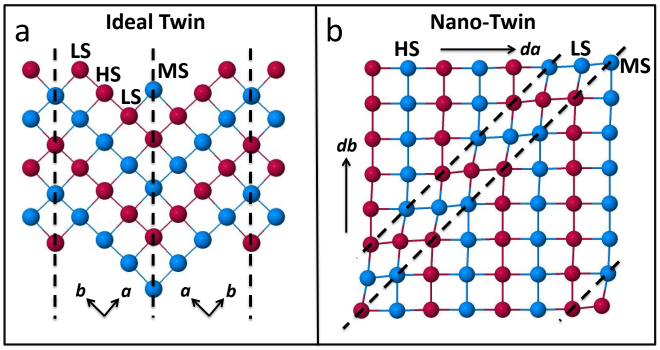

FIG. 2: (Color online) (a) Twin boundary, without strain, separated by three Fe layers. (b) Nanotwin with boundary ⊥ to (110), where atom positions in a distorted cell are barycentric weights of the cell corners. HS, MS and LS are indicated.

scattering near AFM wavevectors, giving 2-dimensional spin fluctuations. Twins also create stripes of increased diamagnetic response,[34] and nucleated SC at magnetic defect boundaries.[35] Niedziela *et al.*[36] proposed that a high density of *nano*twins in the a–b plane from local lattice distortions can improve the agreement between simulated and their measured pair-distribution functions (PDF). Local fluctuating, magnetic-structural variation introduces nanoscale AFM domains (coupling spin and lattice degrees of freedom), potentially lowering the average static moments. Thus, properties of magnetic planar defects (low-energy defects of the SDW), and related spatial/temporal averaging to estimate "ordered" moments, are critical to compare with scattering assessments.

Here we use DFT to simulate various magnetic planar defects, i.e., two types of APBs, a 90^o DB, twin boundaries, and modified "nanotwin," which are low-energy excitations of the SDW. Figure 1a and 1b shows two APB boundaries in the Fe-plane – parallel to the *bc*- or *ac*-planes – and an unstrained 90^o DB is shown in Fig. 1c. Figure 2a shows a typical example of an ideal twin. A modified *nano*twin with 2-dimensional structural distortion (consistent with that suggested by Niedziela *et al.*[36]) is shown in Fig. 2b with a series of static displacements along $a-$ and $b-$axis in the supercell. The undisplaced nanotwin with 1-layer of Fe separating defect planes is really a magnetic stacking fault (SF); a nanotwin supercell has very different boundary conditions than a twin, with different far neighbors and distances between defect pairs; indeed, "ideal twin" supercells formed with 1-layer separation between defect planes (a high density of SFs) has local environments like the nanotwin, except that twin has symmetric relaxations governed by the supercell periodicity, whereas the nanotwin has asymmetric, localized distortions to match the PDF. While we show the defect energies are similar, a nanotwin, due to its boundary condition and supercell, may be considered a fluctuating twin nuclei, which can have low-spin Fe-sites unavailable in the ideal twin supercell.

For nondefected (parent) and defected cells we calculate energy per atom and the associated magnetic moments (bulk moment is 1.6 μ_B), and, hence, the planar defect energy, γ, defined as $\gamma = (E_{\rm def} - E_0)d/V$, where $E_{\rm def}$ and E_0 are the total *energy per atom* of the defected and nondefected cell, respectively. d is the distance between defect planes and V is the volume per atom. While the energy per atom is helpful, γ is the appropriate comparison for cost of creating the defect interface and its dependence on defect density and defect volume.

To do this, we use VASP[37] with plane-wave pseudopotential projected augmented wave (PAW) basis,[38] with an energy cut-off of 380–420 eV. A Monkhorst-pack Brillouin zone integration with a 16^3 **k**-mesh is used for the SDW ($Fmmm$) structure. Smaller **k**-meshes are used for supercells depending on the length along each axis.

For APBs, we constructed doubled (2×1×1), quadrupled, and octupled supercells to examine excitations, denoted by 2-APB, 4-APB and 8-APB, respectively (Fig. 3). For APBs (Figs. 1a,b), we use measured lattice parameters[1] (a=5.6146, b=5.5742 and c=12.9453 Å). For a 90^o DB, we set $\bar{a} = \bar{b} = (a+b)/2 = 5.5944$ Å to reduce strain effects, and construct supercells similar to the APBs, denoted as 2-DB, 4-DB, and 8-DB. Twin ($4[1+n]\times2\times1$) supercells (n=0, 1, ...) are denoted by ($3+4n$)-N Fe-layers between defect planes, and have $4(1+n)$ unit cells along a and $8(1+n)\times10$ atoms/cell. Nanotwin supercells are denoted 5-N, 9-N, and 13-N for Fe-layers between isolated nanotwin pairs; the supercells with the static displacements suggested by Niedziela *et al.* are more complex because the local distortions must be compensated within the cell (Fig. 2b).

The energies and moments for APB and DB defects relative to the non-magnetic (NM) state are shown in Fig. 3 (top), and compared to the AFM ground state (SDW). In all cases, Fe moments have two behaviors: a high-spin state (HS in Fig. 1) at sites away from boundaries and a low-spin state (LS in Fig. 1) at/near boundaries. For APB(bc), the LS moment falls substantially to 0.8 μ_B from 1.6 μ_B, similar to that found by Yin *et*

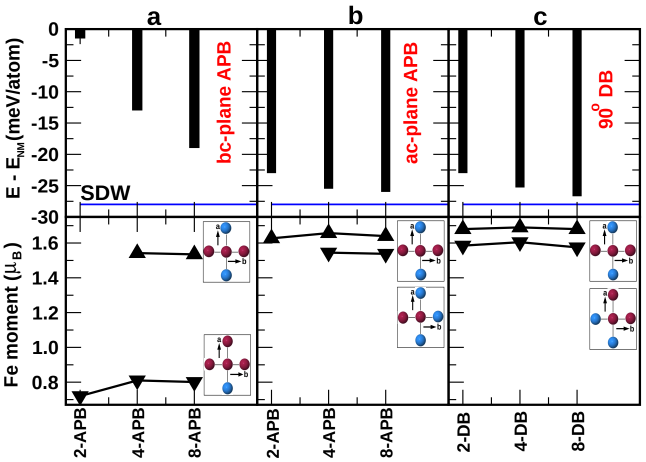

FIG. 3: (Color online) Energies relative to NM state (top) and Fe moments (bottom) for APBs (labels defined in text) in the (a) bc-plane (b) ac-plane, and (c) 90^o DB. SDW indicates the AFM ground state. Insets depict the local Fe environment.

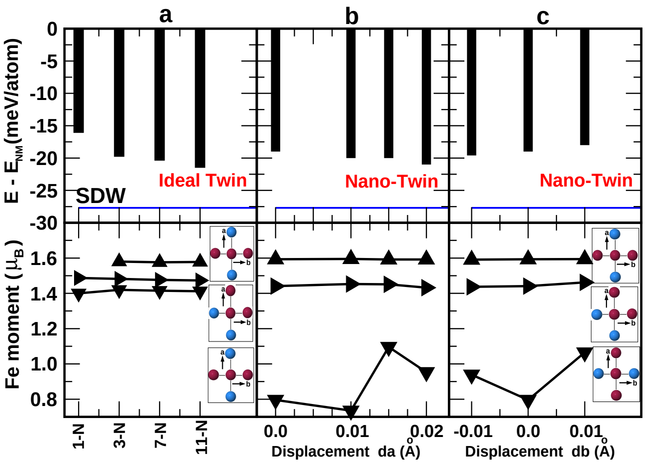

FIG. 4: (Color online) Same as Fig. 3 but for (a) twins (labels defined in text), and nanotwins ($3{\times}3{\times}2$ supercell) with displacements along (b) da and (c) db axes. Fe has HS, MS, and LS states due to local environment (insets).

al.[39] While for APB(ac), the LS moment decreases only to 1.54 μ_B. Moments do not vary much with the size of the supercells, but these two structures energetically compete with the ground state SDW (≤ 9 meV/atom). The two spin states depend on local magnetic environments (inset Fig. 3). For 90^o DB (Fig. 1c), the HS state has a higher moment of 1.7 μ_B due to global strain from changed lattice parameters. The LS moment decreases slightly to 1.57 μ_B near the boundary. The local environment does not play a significant role, suggesting simple models such as counting the number of aligned neighbors is not sufficient to characterize the moments. This defect requires within 2 meV/atom excess energy to form compared to the SDW. They are energetically competing with the APB(ac). Both defects are then expected to be present at the same temperature.

The energy and moments for twins are shown in Fig. 4a. Interestingly, an Fe-atom in a twin has three spin states depending on the local environment. Fe-atoms at the boundary remain in a medium-spin state (MS in Fig. 2a). A LS state occurs on Fe-sites adjacent to the boundary (Fig. 2a). These Fe-sites have the same nearest-neighbor environment as the bulk HS states but differ in the farther neighbors. These defects can form at a few meV/atom, albeit γ is more critical, see below.

The nanotwin energies and moments versus distortion along $a-$ and $b-$axis (in Å unit) are shown in Fig. 4(b,c). Similar to twins, there are three Fe spin states: a HS bulk state (1.6 μ_B), a MS state (1.42 μ_B) at the boundary, and a LS state ($0.8 - 1.0$ μ_B) in the vicinity of the distorted side of the boundary. The structural perturbations show a stronger effect on the LS moments near defect boundaries, decreasing to as low as 0.8 μ_B. Isolated (fluctuating) nanotwins are equally competitive to form as dense twins but with much reduced moments. Energies are affected mostly by the changed magnetic configurations and very little by distortions. So, magnetic defects drive the short-range structural distortion (not the other way around) and can help quench magnetization.

Table I compares the various planar defect energies. Small APB-ac, 90^o-DB, and isolated nanotwin defects (low-energy spin excitations) compete with widely separated twins (spin kinks), which are observed. Energetically, APB(ac) and 90^o DB are the most favorable and most likely to persist after annealing, but twins form and are stabilized by lattice strain from disclinations from twins oriented in the two independent directions.[33] Such small fluctuating defects will affect the observed average moments, whereas separated twins will affect the magnetic correlation length. Planar defect energies (γ in Table I) give the relative *order in which magnetic defects can form and remain after processing*. Structural defects can act as pinning sites for magnetic domain walls.

Strikingly, separated twins are higher in energy than dense twins, until a separation of 16 unit cells (15 Fe-layers), where γ_{twin} reaches a maximum (Table I), after which there is a slow convergence of γ_{twin} versus d (Fig. 5 and [40]). At 28 unit cells ($\sim$11 nm), γ_{twin} has not yet converged; at best convergence could be reached at 32 unit cells ($\sim$13 nm), more likely larger – depending on if γ drops near that of densely packed twins. Observed structural twins[30,31] are extended well beyond the ones computationally possible. Twin separation 'd' is affected by stress, where equilibrium is reached with applied stress roughly $\gamma_{\text{twin}}d$. Also, in real samples twins appear in 90^o oriented pairs, reducing strain at the cost of increased 'd'. While separation will depend on local defects and stress, the average distance 'd' between magnetic twins (estimated from Fig. 5 at 32+ unit cells) should yield a peak in the magnetic susceptibility. Indeed, the measured magnetic correlation length is $\sim$30 unit cells.[30,31] We suggest that small, low-energy excitation can reduce average

TABLE I: γ (2γ for twins) for various planar defects (in $m\mathrm{J/m^2}$). Energies (meV/atom) are relative to SDW. γ_{twin} is dominated by d increasing faster than the decrease in $(E_{\mathrm{def}} - E_0)$, unlike for APBs or DBs.

defect type	supercell	energy	(2)γ
APB (*bc*-plane)	2-APB	26.5	118
	4-APB	15.0	133
	8-APB	9.0	160
APB (*ac*-plane)	2-APB	5.0	22
	4-APB	2.5	22
	8-APB	2.0	35
90^o DB	2-DB	5.0	22
	4-DB	2.7	24
	8-DB	1.3	22
"twin" (ideal)	0-N	18.3	57
"twin" (relaxed)	1-N	9.9	62
"twin" (ideal)	1-N	11.9	74
twin (ideal)	3-N	8.2	102
	7-N	6.6	165
	11-N	6.1	228
	15-N	5.0	(max) 252
	19-N	3.7	231
	23-N	3.0	222
	27-N	2.4	210
nanotwin (undistorted)	3-N	9.2	86
	5-N	6.4	80
	9-N	4.1	77
	13-N	2.5	63
NM bulk	10 atom	28.0	*n/a*

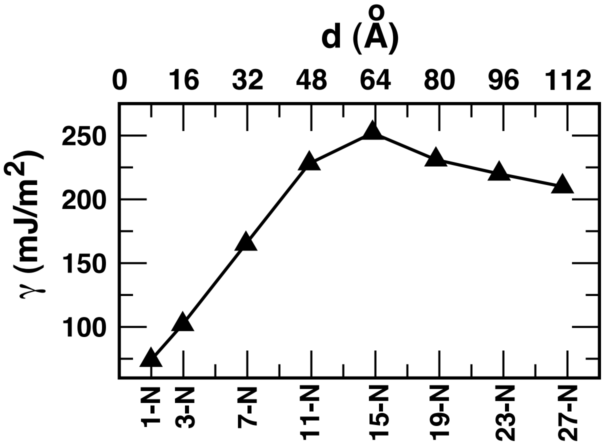

FIG. 5: Twin energy versus number of Fe-layers separating twins, or distance between twin planes.

moments by spatial and temporal averaging, while the twins dictate the magnetic correlation length.

A nanotwin (Fig. 2b) with no local structural distortion is like an isolated, ideal defect pair, not a dense set of twins. To understand the effect of short-ranged structural distortion, we have studied a 1-N ideal twin with(out) relaxation in *ab*-plane for only those atoms near the boundary, more localized than in the nanotwin supercell. The planar defect energy with(out) relaxation is 62 (74) $m\mathrm{J/m^2}$. The relaxation along *a*- and *b*-axis lie within 0.9% of the ideal case, close to the best fit to measured PDF,[36] so the twin and nanotwin are very similar in energy and local structure. However, a nanotwin may be considered a fluctuating twin nuclei, which has many more LS sites (Fig. 4) not available in a twin supercell. Unlike for ideal twins, the nanotwin surface energy decreases to its limiting value as the nanotwin-nanotwin distance grows. For insight into an electronic origin of these magnetic effects we have calculated the Fe-site projected density of states (see [40]).

In summary, we have studied competing low-energy magnetic planar defects in $\mathrm{BaFe_2As_2}$. The favorable defects are APB(*ac*), 90^oDB, and nanotwins, but twins (as observed) are favorable on a longer length scale. The most pronounced reductions in Fe-moment are near the boundaries of APBs(*bc*) and dense twins. We find that isolated closely-spaced twins are energetically favorable and correspond to a recently proposed[36] nanotwin suggested to match the PDF from experiment. The low-energy defects in the perfectly ordered SDW, and the associated spatial and temporal averaging to estimate the "ordered" moments, are critical for comparison to experimental estimates, and serve as a possible explanation for the discrepancy between the Fe moments predicted by DFT ($1.6 - 1.9\ \mu_B$) and experiment ($0.8 - 2.1\ \mu_B$).

In DFT there is no global quenching of Fe-moments, rather quenching is localized near defect boundaries, supporting the increased diamagnetic response[34] at boundaries. Four things can reconcile the various results: (i) the sample may have a high density of magnetic nanotwins that yield strong reduction of the average moment; (ii) the low-energy magnetic defects may be weakly mobile, affecting any time averaged value; (iii) magnet defects with fluctuations in the local Fe-As planar spacing impact values of local moment; and/or (iv) the low-energy fluctuations around the SDW have an extended energy window, which is not currently used in scattering experiments to estimate local moments from integrating the susceptibilities. Indeed, the local moment in $\mathrm{CaFe_2As_2}$ ($0.5\ \mu_B$)[41] and $\mathrm{BaFe_2As_2}$ (0.5–$0.8\ \mu_B$)[11] were estimated by integrating up to about 0.1 *e*V, where DMFT suggests ~1 *e*V window.[42] It would be beneficial to adjust the energy window in neutron-scattering to assess this effect on the assessed Fe moments.

Work was supported by the U.S. Department of Energy, Office of Basic Energy Science, Division of Materials Science and Engineering, and by the Center for Defect Physics, an Energy Frontier Research Center at ORNL. Ames Laboratory is operated for the U.S. DOE by Iowa State University under contract DE-AC02-07CH11358.

---

[*] Electronic address: aftab@ameslab.gov; snkhan@illinois.edu, ddj@ameslab.gov

[1] M. Rotter, M. Tegel, and D. Johrendt, Phys. Rev. B **78**, 020503 (2008).

[2] N. Ni *et al.*, Phys. Rev. B **78**, 214515 (2008).

[3] N. Ni *et al.*, Phys. Rev. B **82**, 024519 (2010).

[4] P. L. Alireza *et al.*, J. Phys.: Condens. Matter **21**, 012208 (2009).

[5] K. Kuroki *et al.*, Phys. Rev. Lett. **101**, 087004 (2008).

[6] F. Wang *et al.*, Phys. Rev. Lett. **102**, 047005 (2009).

[7] D. J. Singh and M. H. Du, Phys. Rev. Lett. **100**, 237003 (2008).

[8] S. Ideta *et al.*, Phys. Rev. Lett. **110**, 107007 (2013).

[9] P. Richard *et al.*, Phys. Rev. Lett. **104**, 137001 (2010).

[10] L. W. Harriger *et al.*, Phys. Rev. B **84**, 054544 (2011).

[11] M. G. Kim *et al.*, Phys. Rev. Lett. **109**, 167003 (2012).

[12] J. Guo *et al.*, Phys. Rev. B **82**, 180520(R) (2010).

[13] Chao Cao and Jian-Hui Dai, Chin. Phys. Lett. **28**, 057402 (2011).

[14] K. Seo, B. A. Bernevig, and J. P. Hu, Phys. Rev. Lett. **101**, 206404 (2008).

[15] C. Fang *et al.*, Phys. Rev. X **1**, 011009 (2011).

[16] Mengshu Liu *et al.*, Nature Physics **8**, 376-381 (2012).

[17] P. Dai, J. Hu, and E. Dagotto, Nature Physics **8**, 709-718 (2012).

[18] E. Arturk and S. Ciraci, Phys. Rev. B **79**, 184523 (2009).

[19] M. J. Han *et al.*, Phys. Rev. Lett. **102**, 107003 (2009).

[20] D. J. Singh, Phys. Rev. B **78**, 094511 (2008).

[21] Q. Huang *et al.*, Phys. Rev. Lett. **101**, 257003 (2008).

[22] S. D. Wilson *et al.*, Phys. Rev. B **79**, 184519 (2009).

[23] H. Gretarsson *et al.*, Phys. Rev. B **84**, 100509(R) (2011).

[24] P. Vilmercati *et al.*, Phys. Rev. B **85**, 220503 (2012).

[25] S.-H. Baek *et al.*, Phys. Rev. B **79**, 052504 (2009).

[26] V. I. Anisimov *et al.*, J. Phys.: Condens. Matter **21**, 075602 (2009); Physica C **469**, 442-447 (2009).

[27] J. Wu *et al.*, Phys. Rev. Lett. **101**, 126401 (2008).

[28] Huaixiang Huang, *et al.* , Phys. Rev. **B 83**, 134517 (2011).

[29] I.I. Mazin and M.D. Johannes, Nature Physics **5**, 141-144 (2008).

[30] M.A. Tanatar *et al.*, Phys. Rev. B **79**, 180508(R) (2009).

[31] C. Ma *et al.*, Phys. Rev. B **79**, 060506(R) (2009).

[32] M.A. Tanatar *et al.*, Phys. Rev. B **81**, 184508 (2010).

[33] A.H. King and Yimei Zhu, Phil. Mag. A, **67**, 1037-1044 (1993).

[34] B. Kalisky, *et al.*, Phys. Rev. B **81**, 184513 (2010).

[35] H. Xiao, *et al.*, Phys. Rev. B **85**, 0224530 (2012).

[36] J.L. Niedziela, M.A. McGuire, and T. Egami, Phys. Rev. B **86**, 174113 (2012).

[37] G. Kresse and J. Furthmüller, Phys. Rev. **B 54**, 11169 (1996); Comput. Mat. Sci. **B 6**, 15 (1996).

[38] G. Kresse and D. Joubert, Phys. Rev. **B 59**, 1758 (1999).

[39] Z. P. Yin and W. E. Pickett, Phys. Rev. B **80**, 144522 (2009).

[40] See Supplemental Material at [URL] for details of (i) long-range nature of γ_{twin} convergence vs. number of Fe-layers separating twins, and (ii) the l-projected Fe-DOS.

[41] S. O. Diallo *et al.*, Phys. Rev. B **81**, 064505 (2010).

[42] A. Toschi *et al.*, Phys. Rev. B **86**, 064411 (2012).